Heliyon 10 (2024) e33606

Contents lists available at ScienceDirect

Heliyon

journal homepage: www.cell.com/heliyon

Research article

Solid state synthesis of lead-free Sm-doped $Na_{0.5}Bi_{4.5}Ti_4O_{15}$ ceramics for enhanced dielectric and electrical properties

Fida Rehman [a,b,**], Pervaiz Ahmad [c,e,*], Atta Ur Rahman [a], Abdulrahman I. Alharthi [d], Awais Khalid [e], Mohammad Rashed Iqbal Faruque [f], Abdul Hakim Shah [a], Mshari A. Alotaibi [d], Hazrat Ali [g], Hamid Osman [h], Mayeen Uddin Khandaker [i,j]

[a] Department of Physics, Khushal Khan Khattak University, Karak, KP, Pakistan
[b] School of Materials Science and Engineering, Beijing Institute of Technology, Beijing, 100081, China
[c] Department of Physics, University of Azad Jammu and Kashmir, 13100, Muzaffarabad, Pakistan
[d] Department of Chemistry, College of Science and Humanities, Prince Sattam Bin Abdulaziz University, P.O. Box 173, Al-Kharj, 11942, Saudi Arabia
[e] Department of Physics, College of Science and Humanities in Al-Kharj, Prince Sattam bin Abdulaziz University, Al-Kharj, 11942, Saudi Arabia
[f] Space Science Centre, Universiti Kebangsaan Malaysia (UKM), Bangi, 43600, Selangor, Malaysia
[g] Department of Physics, Abbottabad University of Science & Technology, Havelian, KP, Pakistan
[h] Department of Radiological Sciences, College of Applied Medical Sciences, Taif University, 21944, Taif, Saudi Arabia
[i] Applied Physics and Radiation Technologies Group, CCDCU, School of Engineering and Technology, Sunway University, Bandar Sunway, 47500, Selangor, Malaysia
[j] Faculty of Graduate Studies, Daffodil International University, Daffodil Smart City, Birulia, Savar, Dhaka, 1216, Bangladesh

ARTICLE INFO

Keywords:
$Na_{0.5}Sm_{0.5}Bi_4Ti_4O_{15}$
Dielectric
Aurivillius-ceramics
$Na_{0.5}Bi_{4.5}$
Ceramics

ABSTRACT

Here we report the synthesis of Sm-doped $Na_{0.5}Bi_{4.5}Ti_4O_{15}$ ($Na_{0.5}Sm_{0.5}Bi_4Ti_4O_{15}$) lead-free ceramics via a conventional solid-state technique. Investigations of $Na_{0.5}Bi_{4.5}Ti_4O_{15}$ (NBT) and $Na_{0.5}Sm_{0.5}Bi_{4.5}Ti_4O_{15}$ (NSBT) ceramics were demonstrated in detail to understand the composition-based structure-property of Aurivillius compounds and related functional material. Dielectric properties for frequency and temperature in a wide range were analyzed. The conduction activation energy values of NSBT ceramics are obtained to be 1.40 eV, whereas, the NBT ceramics get the value to be 1.31 eV. At higher temperatures, the conduction activation energy value of NSBT ceramics is 1.32 eV for both frequencies of 100 Hz and 1 kHz, whereas, for NBT compounds, the calculated value is 1.27 eV for both frequencies. The simulation performed on the impedance data for capacitive and resistance elements shows well-fitting curves which indicates a single relaxation behavior in the material. Similarly, the *AC*-conductivity data were analyzed which gives different conduction processes and relaxation activation energies in the NSBT ceramics.

* Corresponding author. Department of Physics, University of Azad Jammu and Kashmir, 13100, Muzaffarabad, Pakistan.
** Corresponding author. Department of Physics, Khushal Khan Khattak University, Karak, KP, Pakistan.
E-mail addresses: fida_Ph@yahoo.com (F. Rehman), pervaiz_pas@yahoo.com (P. Ahmad).

https://doi.org/10.1016/j.heliyon.2024.e33606
Received 4 March 2024; Received in revised form 22 April 2024; Accepted 24 June 2024
Available online 25 June 2024

1. Introduction

The Aurivillius structures are of great interest due to their excellent properties for a variety of applications in modern technology. These compounds have high curie temperatures which can make them useful choices at elevated temperatures. Its fatigue-free behaviors add long life to materials. Similarly, its large spontaneous polarization makes these compounds remarkable materials for various purposes in research and development [1–6]. Aurivillius structures, especially bismuth-based layered structures are famous for their compositional flexibility. These structures ease numerous elemental structural engineering via their general formulation, $A_{m-1}Bi_2B_mO_{3m+3}$, where, *A* represents cation with a 12-coordinate and *B*-cation with a 6-coordinate system [7,8]. ABO_3-perovskite structure and Bi_2O_2-layer sandwiched to make Aurivillius layer structured compounds.

Lead-free compounds are the focus of the latest research of this era. $Bi_4Ti_3O_{12}$ is an emerging Aurivillius compound that has numerous potential applications, especially in the energy sector [9]. Combining $Bi_4Ti_3O_{12}$ with $BiFeO_3$ oxides gives excellent photoelectrochemical properties [10]. Rare-earth doped four-layered Aurivillius compounds give good electrical properties by suppressing the oxygen vacancies which was generated as a result of Bi volatilization in the material [11–13]. Researchers have explored many Na-based potential compounds such as $(Bi_{0.49}Na_{0.49}Ba_{0.02})TiO_3$ [14], $0.98(K_{0.5}Na_{0.5}NbO_3)$-$0.02(Bi_{0.5}Na_{0.5}TiO_3)$ [15], $Na_{0.5}Bi_4La_{0.5}Ti_4O_{15}$ [16], $0.9(Bi_{0.5}Na_{0.5}TiO_3)$–$0.1(PbZr_{0.48}Ti_{0.52}O_3)$ [17]. Sugato Hajra et al. synthesized Eu and Fe-doped $Bi_{0.5}Na_{0.5}TiO_3$ lead-free electronic materials which showed good results [18]. Fortunately, $Na_{0.5}Bi_{4.5}Ti_4O_{15}$ is a potential four-layered Aurivillius compound that has many leading applications such as dielectric, piezoelectric, ferroelectric, and pyroelectric devices [19,20]. Besides their pronounced importance with strong properties, they have a drawback that confines their application. High leakage current is a serious issue for these materials. The reason behind the problem is the bismuth instability. It is reported that at high sintering temperatures, bismuth evaporates easily and leaves behind various defects behaviors in the structure [21–24]. To understand and resolve this issue various techniques were adopted. The elemental engineering approach was a unique approach to handling the issue [25–27].

Our previous studies and a few other reports show good results via substitution of rear-earth elements which can suppress the oxygen vacancies and overcome the defect behaviors [28–32]. The microstructures and defect behaviors have a deep relation/effect on the electrical mechanisms in the ceramics compounds. Therefore, investigations of electrical and dielectric properties are significant to explore the deep understanding of these compounds.

In this study, Samarium (Sm), Sodium (Na), and bismuth (Bi) based Aurivillus Polycrystalline $Na_{0.5}$-$Bi_{4.5}Ti_4O_{15}$ and $Na_{0.5}Sm_{0.5}$-$Bi_4Ti_4O_{15}$ ceramics were synthesized via solid-state reaction. Afterward, electrical and dielectric properties were elucidated along with the impedance and modulus studies in detail. Relaxation behaviors were elucidated and the different conduction mechanisms at low and high-temperature regions were explained in light of activation energies which were calculated by using the famous Arrhenius equation which was analyzed in detail in the conductivity part. Simulation was also performed which matches exactly with the experimental data.

2. Experimental details

2.1. Materials

Commercially available precursor materials without additional purification processes were used. Sodium carbonate (Na_2CO_3), Bismuth oxide (Bi_2O_3), Samarium (III) oxide (Sm_2O_3), and Titanium dioxide (TiO_2) from Sigma Aldrich Germany with a purity of 99.997 % were cautiously weighed in appropriate ratio for the synthesis of $Na_{0.5}Sm_{0.5}Bi_4Ti_4O_{15}$ compound.

The precursor materials (Na_2CO_3, Bi_2O_3, Sm_2O_3, and TiO_2) with a purity of greater than 99.997 % were first weighted and then uniformly mixed in ethanol.

2.2. Synthesis

Easy ceramics processing method a conventional solid-state reaction approach was adopted to synthesize the $Na_{0.5}Bi_{4.5}Ti_4O_{15}$ and $Na_{0.5}Sm_{0.5}Bi_4Ti_4O_{15}$ electroceramics. The weighted raw chemicals were uniformly mixed with the help of a mortar pestle in an ethanol medium. The precursors were thoroughly mixed for 5 h in an open atmosphere to evaporate the ethanol. Further, the fine mixed chemicals were calcined at 750 °C for 150 min. After the calcination process, the furnace was cooled and the material was crushed to a fine flour-like powder. The soft smooth powders were pressed via a hydraulic press of cold pressure 5 x10^6 Nm^{-2} to pellets of size 1 mm in thickness and 10 mm in diameter via steel mold. The Pressurized pellets were heated in a programmed Muffle furnace up to 1100 °C at 4 °C min^{-1} and sintered at 1100 °C for 180 min in an air atmosphere then cooled down to 400 °C at 2 °C min^{-1} and finally cooled down freely to room temperature. The obtained pellets were again ground to fine soft powders and used for different measurements.

2.3. Characterization and measurement

The X-ray diffraction (XRD) patterns were obtained for phase conformation of the material via using a PanAnalytical X'pert material research diffractometer (MRD) and a high-resolution diffractometer (PANalytical B.V., Almelo, Netherlands) with Cu Ka radiation from 5° to 70° ($\lambda = 1.5405$ Å). A microstructure study of the samples was carried out with the help of a scanning electron microscope (SEM) (M/S TESCAN Mira 3, Brno, Czech Republic). Electrical measurements: the synthesized pellets were polished smooth and parallel with emery paper and coated with silver paint (W–662Y-55, Wells Electronics Materials (Shanghai) Co., Ltd) to obtain silver electrodes on both faces. The paint is dried at 160 °C for 27 min and then heated at 760 °C for 23 min to ensure it is

moisture-free. The sample was used for electrical and dielectric properties. Archimedes' principles were used to study the densities of the samples. Dielectric responses of the samples were measured at a temperature range of 30 °C–650 °C using an impedance analyzer (Agilent 4294A) with a wide frequency range and a variable-temperature sample stage.

3. Results and discussion

Structural investigations of $Na_{0.5}Bi_{4.5}Ti_4O_{15}$ and $Na_{0.5}Sm_{0.5}Bi_4Ti_4O_{15}$ samples were carried out with the help of the X-ray diffraction technique (XRD). Fig. 1 represents the X-ray diffraction patron of the as-sintered and Sm-substituted sample. The patron shows that all the diffraction peaks match exactly to the patron of the four-layered Aurivillius compound with no other phase which conforms to the formation of single-phase four-layer structured Aurivillius materials. $Na_{0.5}Bi_{4.5}Ti_4O_{15}$ patron shows matching with the JCPDF card Number 74–1316 which gives a tetragonal structure with lattice parameters, a = 3.846 Å, b = 3.846 Å, and c = 40.708 Å. XRD patron of Sm substituted $Na_{0.5}Bi_{4.5}Ti_4O_{15}$ ceramics is identified to match with the JCPDS card No. 74–1320 which crystalizes in a tetragonal structure. $Na_{0.5}Sm_{0.5}Bi_4Ti_4O_{15}$ ceramics lattice parameters were obtained to be a = 3.8401 Å, b = 3.8401 Å, and c = 40.7502 Å. The $Na_{0.5}Bi_{4.5}Ti_4O_{15}$ compound has a high diffraction peak which represents the dominant diffraction peak of Aurivillius four-layered compounds.

Fig. 2 (a) and (b) shows SEM micrograph and grain size distribution of $Na_{0.5}Sm_{0.5}Bi_4Ti_4O_{15}$ ceramics. The microstructure reveals plat-like grains. These grains are bound closely with fewer holes/spaces, which confirms that the material is packed tight and has low porosity. The sample density was calculated via Archimedes process and found to be ~94 %. The sample shows non-uniform grain sizes in the range 1–4 μm as shown in Fig. 2 (b).

Fig. 3 **(a–d)** shows a dielectric plot of $Na_{0.5}Sm_{0.5}Bi_4Ti_4O_{15}$ and $Na_{0.5}Bi_{4.5}Ti_4O_{15}$ compounds in a diverse range of frequency and temperature. Fig. 3 (**a**) and (**b**) demonstrate that the dielectric real and imaginary curves in the $Na_{0.5}Sm_{0.5}Bi_4Ti_4O_{15}$ ceramics increase slowly below 300 °C and 200 °C for real and imaginary parts respectively. While a rapid change was observed above these temperatures. Dielectric dispersion in Fig. 3 (a) and Fig. 3 (b) was observed in the range ~ 340 °C–400 °C. At ~590 °C, the peak may be owed to the phase transition. Fig. 3 (**c**) and (**d**) present the dielectric curves of NBT ceramics which give a dielectric peak above 500 °C.

The ferroelectric to paraelectric transition of $Na_{0.5}Bi_{4.5}Ti_4O_{15}$ compounds was observed at 655 °C confirmed in various reports [33, 34]. The abnormal peaks observed in the low-temperature region in the imaginary dielectric of $Na_{0.5}Bi_{4.5}Ti_4O_{15}$ compounds which is frequency frequency-dependent due to the space charges relaxation mechanism in the material. Previous reports show that doping of Lanthanum in $Na_{0.5}Bi_{4.5}Ti_4O_{15}$ occurred at about 580 °C. It is indicated that rare-earth elements doping in the Aurivillius family can decrease the phase transition temperature [35,36].

Fig. 4 (a – d) shows $Na_{0.5}Sm_{0.5}Bi_4Ti_4O_{15}$ and $Na_{0.5}Bi_{4.5}Ti_4O_{15}$ ceramics real and imaginary permittivity plots. **Figure (a)** and **(b)** gives a slow decrease of real and imaginary curves with increasing frequency. Fig. 4 (a) shows that at $f > 10^4$ Hz, a Pluto region is observed which is frequency-independent. The loss factor ε" was decreased with frequency increase. The grain boundaries offered high resistance therefore a large amount of energy is needed to give movement to the charge at a low-frequency side. Hence loss will be observed in this area. Similarly, less energy is needed to give motion to charges present at high-frequency regions, so less loss in energy will be observed. Fig. 4 (c) and **(d)** present dielectric curves that show a decrease in both real and imaginary with increasing frequency of NBT ceramics. One can observe a dispersion region (marked with an arrow) at the NBT sample in Fig. 4 (d).

Fig. 5 (a) and **(b)** present impedance plots of $Na_{0.5}Sm_{0.5}Bi_4Ti_4O_{15}$ Compound. The $-Z''$ vs Z' plots give a semicircular arc. The semicircular arc diameter elucidated the resistance of the synthesized materials. The real and imaginary curves of $-Z''$ vs Z' gives semicircular arcs and its diameter shows the resistance of the materials. The interception on the horizontal (Z'-axis) is observed to decrease with the rise of temperature which suggests that the resistance of the material is decreased with temperature increase.

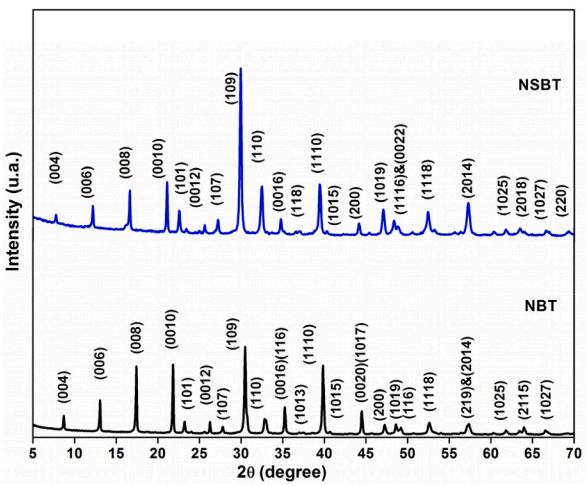

Fig. 1. XRD pattern of $Na_{0.5}Sm_{0.5}Bi_4Ti_4O_{15}$ (NSBT) and $Na_{0.5}Bi_{4.5}Ti_4O_{15}$ (NBT) ceramics.

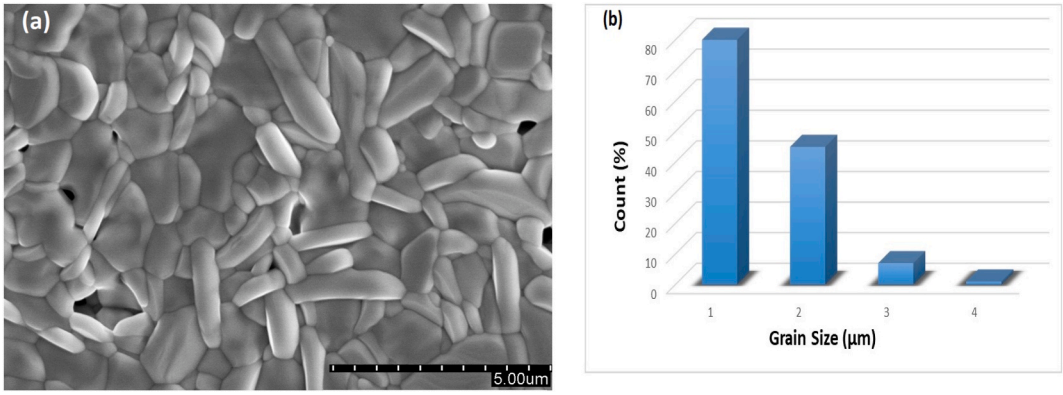

Fig. 2. **(a)** Scanning electron micrograph **(b)** grain size distribution of NSBT ceramics.

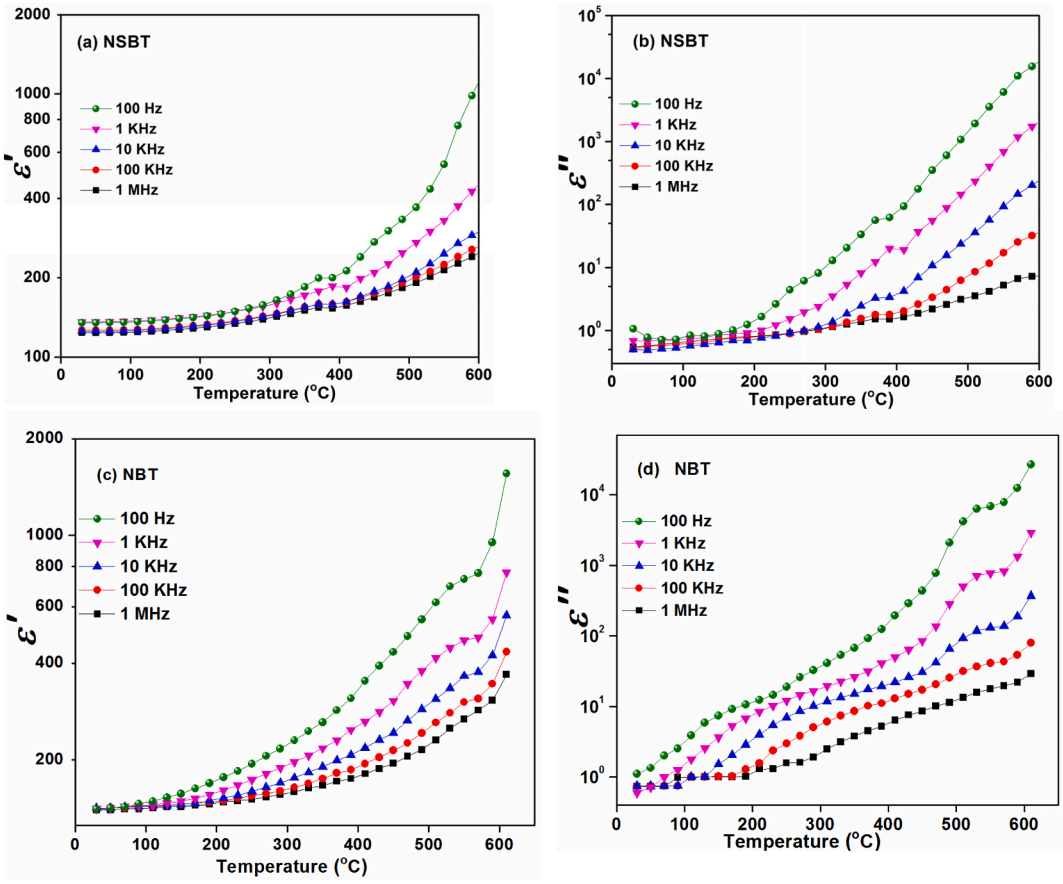

Fig. 3. (a), and **(b)** show the dielectric real and imaginary curves in the $Na_{0.5}Sm_{0.5}Bi_4Ti_4O_{15}$ ceramics, whereas, **(c)** and **(d)** are the dielectric real and imaginary curves of $Na_{0.5}Bi_{4.5}Ti_4O_{15}$ ceramics.

Simulation results of impedance data at 530 °C are given in Fig. 5 (b). The simulation was carried out with the equivalent circuit, consisting of Resistance, capacitance, and phase constant. The simulation performed on the impedance data shows well-finting curves which indicates a single relaxation behavior in the material. The obtained calculation values of the simulation are depicted in Fig. 5 (b). Table 1 shows the obtained calculation values of equivalent circuit elements. whereas, the *n* value for perfect resister and ideal capacitor are "0" and "1" respectively [37].

Fig. 6 shows frequency-dependent modulus curves at a wide range of temperatures i.e. 370 -650 °C. The plots present a gradual increase at low frequency which leads to a sharp peak. It can be observed that a further increase in frequency causes a gradual decrease

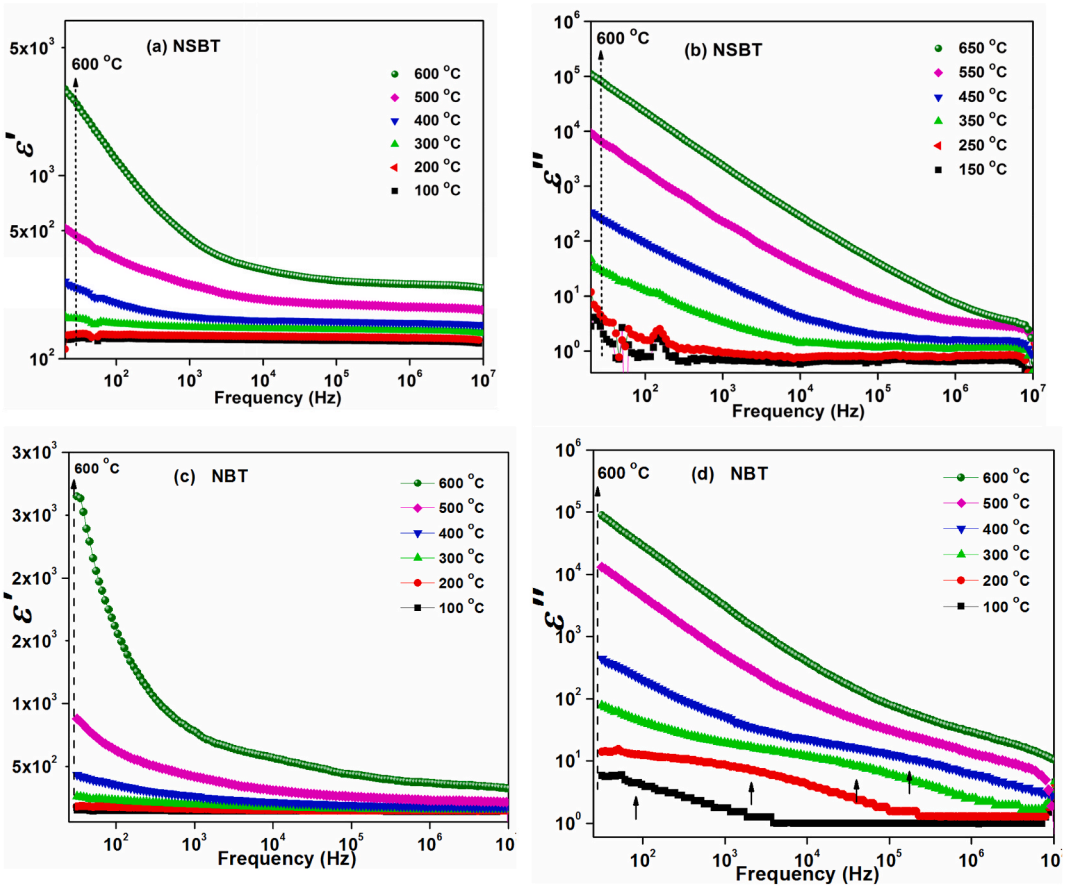

Fig. 4. (a) and **(b)** are real $\mathcal{E}'$ and imaginary $\mathcal{E}''$ parts of NSBT, whereas, **(c)** and **(d)** of NBT compounds.

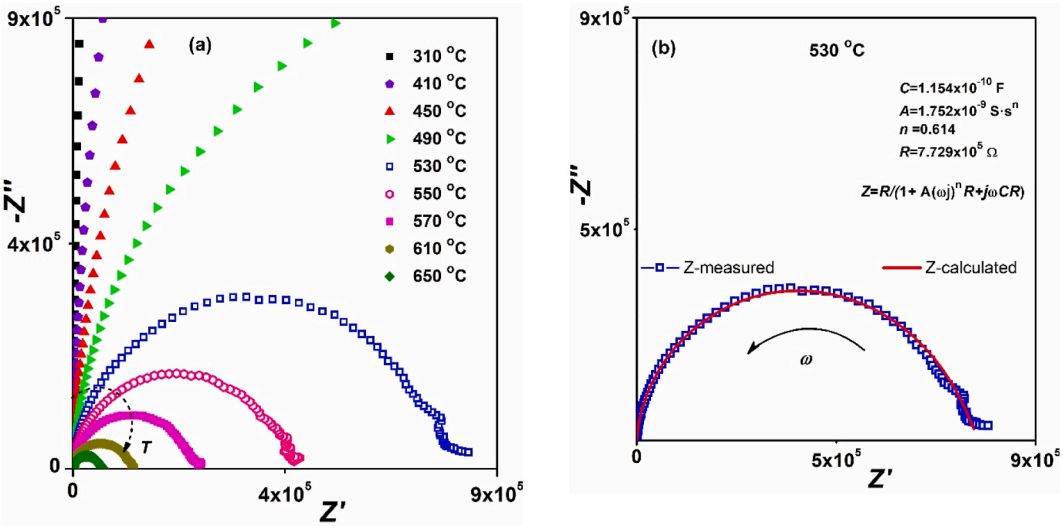

Fig. 5. (a) Cole-Cole plots, and **(b)** Simulation curve of NSBT ceramics at 530 °C with an equivalent circuit. The solid-colored line is the fitting curve.

Table 1
The obtained calculation values of equivalent circuit elements.

C	R	A	n
1.155×10^{-10} F	7.728×10^{5} Ω	1.752×10^{-9} S.s^{n}	0.614

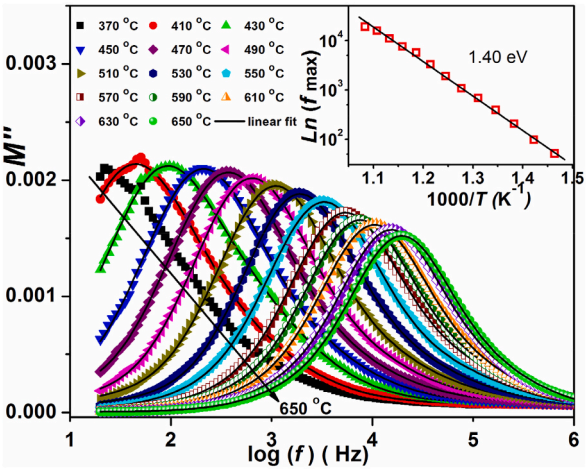

Fig. 6. Modulus plots at various temperatures of NSBT samples. Gaussian fitting solid lines are shown with solid lines, Relaxation frequency vs temperature curve of NSBT compound is shown in the inset.

in the curves. The changing peak position is noted in the modulus curves to high frequency with temperature increase. It is observed that the curve's maxima decrease with temperature rise. This shows an increase in capacitance values of the ceramics given as $\frac{M''_{max}}{\varepsilon_o} = \frac{1}{2c}$ [38]. Further, the modulus plots conform to a single relaxation peak in the ceramics which is in equivalence to the impedance results. The Inset of Fig. 6 gives relaxation frequency as a function of the inverse of temperature. Arrhenius's famous formula $f^r = f_o \exp(-E_a/K_B T)$ helped in the calculation of the relaxation activation energies and the obtained value is almost 1.4 eV.

The insets give $\ln(\sigma_{dc})$ as a function of temperature.

Fig. 7 (a), and **(b)** give *AC*-conductivity plots at different temperatures. In the conductivity plots, there are two different behaviors, one is frequency-dependent and the other is frequency-independent. The low-temperature curves show a frequency-dependent nature while the high-temperature lines are independent of frequency. The Plateau region which is frequency independence suggests the dominant nature of DC conductivity. $\ln(\sigma_{dc})$ *vs* $10^3/T$ curves are presented in the inset of Fig. 7 (a) and **(b)**. The analysis of the curves in the insets gives two different slops which indicate two different conduction processes in the ceramics. The conduction activation energy values of NSBT ceramics are obtained to be 1.40 eV, whereas, the NBT ceramics get the value to be 1.31 eV.

The *AC*-conductivity plots of both NSBT and NBT compounds at 100 Hz and 1 KHz are given in Fig. 8 (a) and **(b)**. The curves show that the conductivity values of the compounds increase with increasing temperature and sharp alteration in the conductivity was observed at a high temperature region. Several slops were observed in the curves of *AC* conductivity. This shows different kinds of conduction processes in the materials. The plots in Fig. 8 (a) show three different regions in low, intermediate, and high-temperature regions in NSBT ceramics. Similarly, in NBT ceramics two different regions are observed in low and high-temperature regions as shown in Fig. 8 (a). The activation energy for NSBT ceramics at low-temperature regions was found to be 0.04 eV and 0.05 eV for 100 Hz and 1 KHz respectively. The conduction-activated energy for the intermediate region was obtained as 0.59 eV and 0.56 eV for 100 Hz and 1 KHz respectively. At higher temperatures, the conduction activation energy value of NSBT ceramics is 1.32 eV for both frequencies of 100 Hz and 1 kHz.

The conduction activation energies for the NBT compounds at various temperatures are given in Fig. 8 (b). At high-temperature regions, the calculated value is 1.29 eV for both frequencies. The conduction-activated energy for the intermediate region was obtained as 0.36 eV and 0.43 eV for 100 Hz and 1 KHz respectively. At low-temperature regions, the calculated values are 0.26 eV and 0.30 eV for 100 KHz and 1 KHz respectively.

Fig. 9 (a) and **(B)** show capacitance plots for NSBT and NBT compounds at different frequencies. The drastic progress in electrical properties of bismuth-based compounds may be due to the Sm influence in the structure, which improves the density of the compound by reducing the bismuth evaporation from the material. Reduction in bismuth volatilization at high temperatures slows down the formation of oxygen vacancies in the compounds and improves the dielectric constant [39]. The generation of oxygen vacancies in bismuth-contained compounds is through the following way [40]:

$$Vac_o \Leftrightarrow Vac_o^{\cdot} + e' \qquad Vac_o^{\cdot} \Leftrightarrow Vac_o^{\cdot\cdot} + e'$$

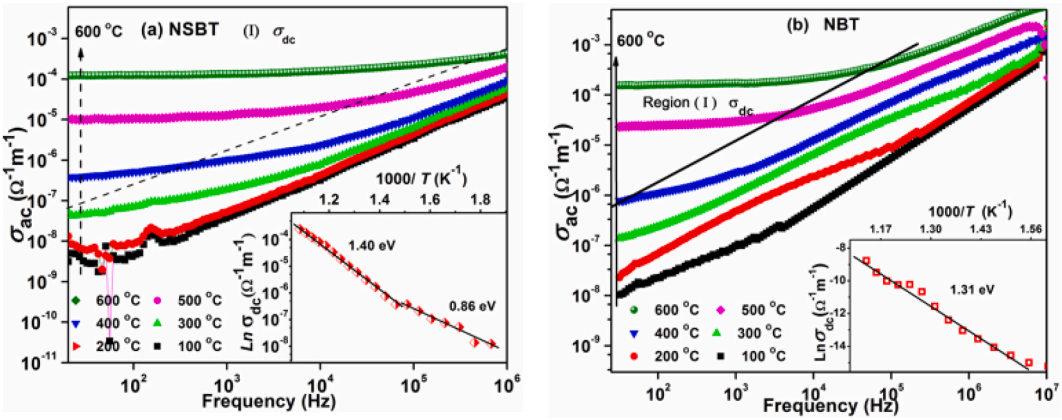

Fig. 7. *AC*-conductivity (σ_{ac}) of **(a)** NSBT, and **(b)** NBT samples at various temperatures.

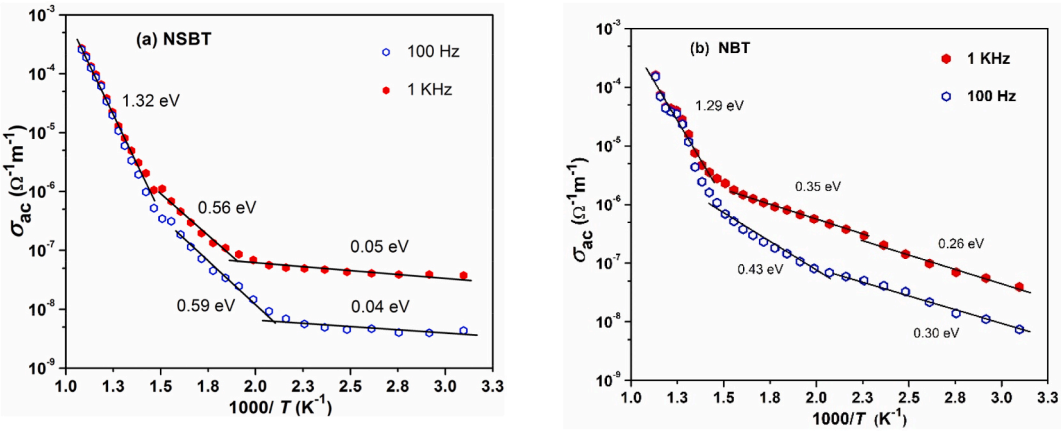

Fig. 8. *AC*-conductivity of **(a)** NSBT and **(b)** NBT compounds at 100 Hz and 1 KHz.

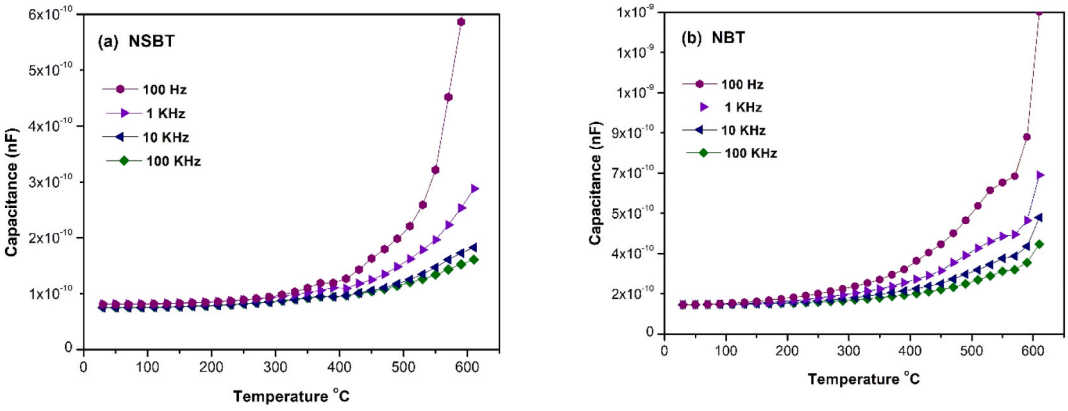

Fig. 9. Capacitance as a function of temperature of (a) NSBT and (b) NBT ceramics at various frequencies.

Vac_o is 1st ionized oxygen vacancy and $Vac_o^{\cdot}$ 2nd ionized oxygen vacancy. These oxygen vacancies can jump due to their movement in the existing electric field. These vacancies jump to assemble in spaces having low free energy like that in grain boundaries. Gathering of these oxygen vacancies in the grain boundaries sites roots realm pinning and consecutively bound polarization switching in the compound [40–42].

Fig. 10 gives plots of Z''/Z''_{max} and M''/M''_{max} as a function of the frequency of NSBT and NBT ceramics at 630 °C. The analysis of

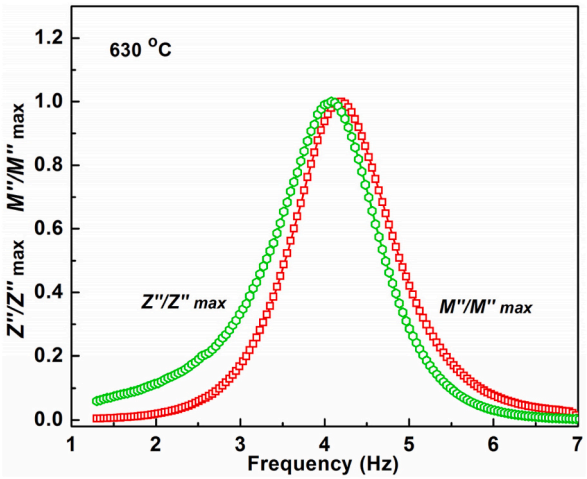

Fig. 10. Z''/Z''_{max} and M''/M''_{max} vs frequency of NSBT samples at 630 °C.

the impedance and modulus curves reveals a single relaxation peak which is in sequence with the single relaxation observed in Figs. 5 and 6 respectively.

4. Conclusions

It has been found that the dielectric real and imaginary curves in the $Na_{0.5}Sm_{0.5}Bi_4Ti_4O_{15}$ ceramics increase slowly below 300 °C and 200 °C for real and imaginary parts respectively, whereas a rapid change was observed above these temperatures. Dielectric dispersion was observed in the range of ~340–400 °C. Conduction and relaxation activation energies were deducted from the data. The simulation performed on the impedance data shows a single relaxation behavior in the material. The doping of Sm is found to improve the density of the compound by reducing the bismuth evaporation from the material at high temperatures. Reduction in bismuth volatilization at high temperatures slows down the formation of oxygen vacancies in the compounds and improves the dielectric constant. These results are useful for understanding the composition-based structure-property relation of Aurivillius compounds and related functional material.

Ethics approval

The manuscript has not been published.

Consent to participate and publication

The authors consent to participate and publication.

Availability of data and materials

The data and materials used in the research are given in the manuscript.

Funding

This research was funded by Fundamental Research Grant Scheme (FRGS), MOE, Malaysia, Code: FRGS/1/2022/TK07/UKM/02/22. The authors extend their appreciation to Taif University, Saudi Arabia, for supporting this work through project number (TU-DSPP-2024-42).

CRediT authorship contribution statement

Fida Rehman: Writing – review & editing, Writing – original draft, Validation, Methodology, Investigation, Formal analysis, Data curation, Conceptualization. **Pervaiz Ahmad:** Writing – original draft, Validation, Supervision, Resources, Methodology, Investigation, Funding acquisition, Data curation, Conceptualization. **Atta Ur Rahman:** Visualization, Validation, Methodology, Investigation, Data curation, Conceptualization. **Abdulrahman I. Alharthi:** Visualization, Validation, Software, Resources, Project administration, Methodology, Investigation, Formal analysis. **Awais Khalid:** Visualization, Validation, Software, Methodology, Investigation, Formal analysis, Data curation, Conceptualization. **Mohammad Rashed Iqbal Faruque:** Visualization, Validation, Software, Project

administration, Investigation, Funding acquisition. **Abdul Hakim Shah:** Validation, Software, Methodology, Investigation, Data curation. **Mshari A. Alotaibi:** Validation, Software, Resources, Investigation, Formal analysis, Data curation, Conceptualization. **Hazrat Ali:** Validation, Software, Resources, Investigation, Formal analysis, Data curation, Conceptualization. **Hamid Osman:** Conceptualization, Funding acquisition, Project administration, Resources, Software, Validation, Visualization. **Mayeen Uddin Khandaker:** Supervision, Software, Resources, Project administration, Methodology, Investigation, Formal analysis, Conceptualization.

Declaration of competing interest

The authors declare that they have no known competing financial interests or personal relationships that could have appeared to influence the work reported in this paper.

Acknowledgements

This research was funded by Fundamental Research Grant Scheme (FRGS), MOE, Malaysia, Code: FRGS/1/2022/TK07/UKM/02/22. The authors extend their appreciation to Taif University, Saudi Arabia, for supporting this work through project number (TU-DSPP-2024-42).

References

[1] H. kodama, F. izumi, A. watanabe, New members of a family of layered bismuth compounds, J. Solid State Chem. 36 (1981) 349–355.
[2] E.C. Subbarao, Ferroelectricity in $Bi_4Ti_3O_{12}$ and its solid solutions, Phys. Rev 122 (1961) 804–807.
[3] Q. Wu, X.H. Chen, L. Zhao, Y.S. Zhao, Y.P. Zhou, S. Zhao, The relaxor properties and energy storage performance of Aurivillius compound with different number of perovskite-like layers, J. Alloy and compd. 911 (2022) 165081.
[4] C.M. Wang, J.F. Wang, S. Zhang, T.R. Shrout, Electromechanical properties of A site (LiCe)-modified sodium bismuth titanate ($Na_{0.5}Bi_{4.5}Ti_4O_{15}$) piezoelectric ceramics at elevated temperature, Appl. Phys. 105 (2009) 094110.
[5] T P Wendari Zulhadjri, M. Ikhram, Y.E. Putri, U. Septiani, Imelda, Enhanced dielectric and ferroelectric responses in La^{3+}/Ti^{4+} co-substituted $SrBi_2Ta_2O_9$ Aurivillius phase, Ceram. Int. 7 (2022) 10328–10332.
[6] C. Mitharwal, S. Mishra, G. Paliwal, S. Mittal, S. Mitra, Microstructure and electrical properties of MnO_2 modified $(Ca_{0.4}Sr_{0.6})Bi_4Ti_4O_{15}$ high T_c aurivillius ceramics, Ceram. Int. 47 (2021) 6860–6866.
[7] B. Aurivillus, Mixed bismuth oxide with layer lattices, Structure of $Bi_4Ti_3O_{12}$, Arkiv. Kemi. 1 (1949) 499–512.
[8] T P Wendari Zulhadjri, U. Septiani, S. Arief, Investigation on structure, dielectric and magnetic properties of the four-layer Aurivillius phase $Pb_{1-x}Bi_{3.5+x}Nd_{0.5}Ti_{4-x}Mn_xO_{15}$ prepared via molten salt method, J. Solid State Chem. 292 (2020) 121723.
[9] A Kumar, P Sharma, T Wang, C W Lai, G Sharma, P Dhiman, Recent progresses in improving the photocatalytic potential of $Bi_4Ti_3O_{12}$ as emerging material for environmental and energy applications, J. Ind. Eng. Chem., https://doi.org/10.1016/j.jiec.2024.03.054.
[10] E. Mercadelli, N. Sangiorgi, S. Fabbri, A. Sangiorgi, A. Sanson, Structural, optical, and photo-electrochemical properties of Aurivillius-type layered $Bi_4Ti_3O_{12}$–$BiFeO_3$ oxides, Sol. Energy Mater. Sol. Cell. 267 (2024) 112732.
[11] Y. Jiang, X. Jiang, C. Chen, Y. Chen, X. Jiang, N. Tu, X. Xia, Y. Luo, S. Zhu, Structural and electrical properties of La3+-doped Na0.5Bi4.5Ti4O15-Bi4Ti3O12 inter-growth high temperature piezoceramics, Ceram. Int. 1 (2017) 6446–6452.
[12] F. Rehman, H.B. Jin, C. Niu, A. Bukhtiar, Y.J. Zhao, J.B. Li, Structural, magnetic and dielectric properties of Bi4Nd0.5Gd0, 5Ti3FeO15 ceramics Ceramics International 42 (2) (2016) 2806–2812.
[13] F. Rehman, J.B. Li, I. Ahmad, H.B. Jin, P. Ahmad, Y. Saeed, M. Shafiq, H. Ali, Dielectric relaxation and electrical properties of Bi2.5Nd0.5Nb1.5Fe0.5O9 ceramics, Mater. Chem. Phys. 226 (2019) 100–105.
[14] S. Hajra, S. Sahoo, R.N.P. Choudhary, Fabrication and electrical characterization of $(Bi_{0.49}Na_{0.49}Ba_{0.02})TiO_3$-PVDF thin film composites, J. Polym. Res. 26 (2019) 14.
[15] S.A. Behera, S. Hajra, S. Panda, A. Amanat, P.G.R. Achary, Structural and electrical properties of $0.98(K_{0.5}Na_{0.5}NbO_3)$-$0.02(Bi_{0.5}Na_{0.5}TiO_3)$ ceramics, Journal of Metals, Materials and Minerals 33 (4) (2023) 1894.
[16] F. Rehman, J.B. Li, P. Ahmad, Y. Saeed, H.B. Jin, Dielectric relaxation and electrical properties of Na0.5Bi4La0.5Ti4O15 electroceramics, J. Electroceram. 44 (2020) 147–153.
[17] M. Sahu, S.K. Pradhan, S. Hajra, B.K. Panigrahi, R.N.P. Choudhary, Studies of structural, electrical, and excitation performance of electronic material: europium substituted 0.9(Bi0.5Na0.5TiO3)–0.1(PbZr0.48Ti0.52O3), Appl. Phys. A 125 (3) (2019) 183.
[18] Sugato Hajra, Arya Tripathy, K. Basanta, Panigrahi[2] and RNP Choudhary[3,] Development and excitation performance of lead free electronic material: Eu and Fe doped $Bi_{0.5}Na_{0.5}TiO_3$ for filter application, Mater. Res. Express 6 (2019) 076304.
[19] T. Takenaka, Gotoh, S. Mutoh, T. Sasaki, A new series of bismuth layer-structured ferroelectrics, Jpn. J. Appl. Phys. 34 (1995) 5384.
[20] S. Kumar, K.B.R. Varma, Structural, dielectric and ferroelectric properties of four-layer Aurivillius phase $Na_{0.5}La_{0.5}Bi_4Ti_4O_{15}$, Mater. Sci. Eng. B 17 (2010) 177.
[21] Y.M. Kim, A. Morozovska, E. Eliseev, M.P. Oxley, R. Mishra, S.M. Selbach, T. Grande, S.T. Pantelides, S. Kalinin, A.Y. Borisevich, Direct observation of ferroelectric field effect and vacancy-controlled screening at the $BiFeO_3$/$LaxSr_{1-x}MnO_3$ interface, Nat. Mater. 13 (11) (2014) 1019–1025.
[22] P. Liang, Y. Li, Y. Zhao, L. Wei, Z. Yang, Origin of giant permittivity and high-temperature dielectric anomaly behavior in $Na_{0.5}Y_{0.5}Cu_3Ti_4O_{12}$ ceramics, J. Appl. Phys. 113 (2013) 224102.
[23] S.F. Liu, Y.J. Wu, J. Li, X.M. Chen, Effects of oxygen vacancies on dielectric, electrical, and ferroelectric properties of $Ba_4Nd_2Fe_2Nb_8O_{30}$ ceramics, Appl. Phys. Lett. 104 (2014) 082912.
[24] M. Li, M.J. Pietrowski, R.A. De Souza, H.R. Zhang, I.M. Reaney, S.N. Cook, J.A. Kilner, DC Sinclair, A family of oxide ion conductors based on the ferroelectric perovskite $Na_{0.5}Bi_{0.5}TiO_3$, Nat. Mater. 13 (2014) 31–35.
[25] F. Rehman, H.B. Jin, J.-B. Li, Effect of reduction/oxidation annealing on the dielectric relaxation and electrical properties of Aurivillius $Na_{0.5}Gd_{0.5}Bi_4Ti_4O_{15}$ ceramics, RSC Adv. 6 (2016) 35102.
[26] X. Chen, J. Xiao, J. Yao, Z. Kang, F. Yang, X. Zeng, Room temperature magnetoelectric coupling study in multiferroic $Bi_4NdTi_3Fe_{0.7}Ni_{0.3}O_{15}$ prepared by a multicalcination procedure, Ceram. Int. 40 (2014) 6815–6819.
[27] N.V. Prasad, S.N. Babu, A. Siddeshwar, G. Prasad, G.S. Kumar, Electrical studies on A- and B-site-modified $Bi_4Ti_3O_{12}$ ceramics, Ceram. Int. 35 (2009) 1057–1062.
[28] Rehman Fida, J.-B. Li, P. Ahmed, M.S. Khan, Y. Saeed, A. khan, M. Zubair, Effect of Na doping on dielectric relaxation and conduction behaviors of Aurivillius Na0.5Bi4.5Ti4O15 ceramics, Rare Met. 40 (5) (2021) 1247–1254.
[29] M. Osada, M. Tada, M. Kakihana, T. Watanabe, H. Funakubo, Cation distribution and structural instability in $Bi_{4-x}La_xTi_3O_{12}$, Jpn. J. Appl. Phys. 40 (2001) 5572–5575.

[30] Z. Peng, L. Chen, Y. Xiang, F. Cao, Microstructure and electrical properties of lanthanides-doped $CaBi_2Nb_2O_9$ ceramics, Mater. Res. Bull. 148 (2022) 111670.
[31] F. Huang, X.M. Lu, W.W. Lin, X.M. Wu, Y. Kan, J.S. Zhu, Effect of Nd dopant on magnetic and electric properties of $BiFeO_3$ thin films prepared by metal organic deposition method, Appl. Phys. Lett. 89 (2006) 242914.
[32] J.S. Kim, Effect of Nd dopping on dielectric and ferroelectric properties of bismuth titanate ceramics, Integr Ferroelectr. 79 (2006) 139–145.
[33] D. Gao, K.W. Kwok, D. Lin, Microstructure, piezoelectric and ferroelectric properties of Mn-added $Na_{0.5}Bi_{4.5}Ti_4O_{15}$ ceramics, Curr. Appl. Phys. 11 (2011) S124–S127.
[34] H. Du, X. Shi, Dielectric and piezoelectric properties of barium-modified Aurivillius-type $Na_{0.5}Bi_{4.5}Ti_4O_{15}$, J. Phys. Chem. Solid. 72 (11) (2011) 1279–1283.
[35] S. Kumar, K.B.R. Varma, Structural, dielectric and ferroelectric properties of four-layer Aurivillius phase $Na_{0.5}La_{0.5}Bi_4Ti_4O_{15}$, Mater. Sci. Eng. B. 172 (2) (2010) 177–182.
[36] F. Rehman, J.B. Li, Y.K. Dou, J.S. Zhang, Y.J. Zhao, M. Rizwan, S. Khalid, H.B. Jin, Dielectric relaxations and electrical properties of Aurivillius $Bi_{3.5}La_{0.5}Ti_2Fe_{0.5}Nb_{0.5}O_{12}$ Ceramics, J. Alloys Compd. 654 (2016) 315–320.
[37] P. Tirupati, S.K. Mandal, A. Chandra, Effect of oxygen annealing on the multiferroic properties of Ca^{2+} doped $BiFeO_3$ nanoceramics, J. Appl. Phys. 116 (24) (2014) 244105.
[38] W. Lei, Y.Y. Yan, X.H. Wang, et al., Improving the breakdown strength of $(Mg_{0.9}Zn_{0.1})2(Ti_{1-x}Mn_x)O_4$ ceramics with low dielectric loss, Ceram. Int. 41 (2015) 521–525.
[39] A.K. Yadav, S Kumar Anita, V.R. Reddy, P.M. Shirage, S. Biring, S. Sen, Structural and dielectric properties of $(Pb_{1-x})(Na_{0.5}Sm_{0.5})_xTiO_3$ ceramics, J. Mater. Sci. Mater. Electron. 28 (14) (2017).
[40] F.A. Kröger, H.J. Vink, in: S. Frederick, T. David Relations (Eds.), Solid State Physics, Between the Concentrations of Imperfections in Crystalline Solids, vol. 3, Academic Press, New York, 1956, pp. 307–435.
[41] Y. Chen, H. Zhou, Q. Wang, J. Zhu, Doping effects in Gd/Cr co-doped Bi_3TiNbO_9 Aurivillius-type ceramics with improved electrical properties, J. Materiomics (2021), https://doi.org/10.1016/j.jmat.2021.12.008.
[42] K. Sunil, K.B.R. Verma, Influence of lanthanum doping on the dielectric, ferroelectric and relaxor behaviour of barium bismuth titanate ceramics, J. Phys. D 42 (2009) 075405.